BRAIN CONNECTIVITY
Volume 2, Number 3, 2012

DOI: 10.1089/brain.2012.0085

# Variable Bandwidth Filtering for Improved Sensitivity of Cross-Frequency Coupling Metrics

Jeffrey I. Berman,[1,2,*] Jonathan McDaniel,[1,2,*] Song Liu,[1] Lauren Cornew,[1] William Gaetz,[1,2] Timothy P.L. Roberts,[1,2] and J. Christopher Edgar[1,2]

## Abstract

There is an increasing interest in examining cross-frequency coupling (CFC) between groups of oscillating neurons. Most CFC studies examine how the phase of lower-frequency brain activity modulates the amplitude of higher-frequency brain activity. This study focuses on the signal filtering that is required to isolate the higher-frequency neuronal activity which is hypothesized to be amplitude modulated. In particular, previous publications have used a filter bandwidth fixed to a constant for all assessed modulation frequencies. The present article demonstrates that fixed bandwidth filtering can destroy amplitude modulation and create false-negative CFC measures. To overcome this limitation, this study presents a variable bandwidth filter that ensures preservation of the amplitude modulation. Simulated time series data were created with theta-gamma, alpha-gamma, and beta-gamma phase-amplitude coupling. Comparisons between filtering methods indicate that the variable bandwidth approach presented in this article is preferred when examining amplitude modulations above the theta band. The variable bandwidth method of filtering an amplitude modulated signal is proposed to preserve amplitude modulation and enable accurate CFC measurements.

**Key words:** amplitude modulation; brain; cross-frequency coupling; functional connectivity

## Introduction

Neuronal activity is related to the rate at which neurons fire and produce action potentials. Groups of neurons increase and decrease their activity in unison and oscillate at various frequencies. When hundreds of thousands to millions of neurons are synchronously active, their electric and magnetic fields are large enough to be measured outside the brain. Strong evidence has shown that communication between brain regions occurs via the temporal synchronization of neural firing (Fries, 2005; Schoffelen et al., 2011).

Distinct frequency bands have been associated with cognitive processes and behavioral states (Başar et al., 2001). The frequency bands are historically termed delta (0 to 4 Hz), theta (4 to 8 Hz), alpha (8 to 12 Hz), beta (12 to 30 Hz), and gamma (>30 Hz). The methods used to examine functional connectivity (FC) both within and between frequency bands include coherence and the phase-locking index (Nunez, 1997; Tallon-Baudry et al., 2001). Recently, signal processing methods have been developed to examine the correlation between the phase of one frequency band and the power of another frequency band (Canolty et al., 2006; Osipova et al., 2008). This interaction between frequency bands is termed cross-frequency coupling (CFC).

CFC is an important area of research, because it can provide insight into how neural networks process and share information. Current and future CFC studies are also motivated by the hypothesis that patterns of CFC are altered in neuropsychiatric disorders. CFC has primarily been investigated using intracranial electroencephalography (EEG) and depth electrodes; however, scalp EEG and magnetoencephalography (MEG) have also been used (Canolty et al., 2006, 2012; Cohen, 2008; Handel and Haarmeier, 2009). For example, resting-state MEG studies have shown gamma power to be phase locked to alpha oscillations, with the strongest relationships observed within the occipital areas (Osipova et al., 2008). Other studies show that phase-amplitude CFC plays a functional role. Sauseng et al. (2008) found that increased theta-gamma CFC was related to visual attention. Tort et al. (2008) reported that theta-gamma CFC is correlated with accuracy on a learning task in rats, and Axmacher et al. (2010) reported associations between the CFC and working memory in humans. Delta to gamma CFC has been linked to the detection of weak sensory signals (Handel and Haarmeier, 2009).

[1]Department of Radiology, Children's Hospital of Philadelphia, Philadelphia, Pennsylvania.
[2]Department of Radiology, Perelman School of Medicine, University of Pennsylvania, Philadelphia, Pennsylvania.
*These two authors have contributed equally and are co-first authors.

Recent studies have also examined CFC with the aim of understanding functional brain abnormalities in psychiatric disorders such as schizophrenia (Kirihara et al., 2012).

A primary feature of CFC is the existence of a higher-frequency signal with amplitude modulations that correlate with the phase of a low-frequency signal. Several methods have been proposed that measure CFC [for a review, see (Tort et al., 2010)]. The present study demonstrates how signal filtering parameters affect the sensitivity of CFC metrics. As detailed in the Background Theory section, amplitude-modulated signals have a complex frequency spectrum with a bandwidth that is related to the frequency of modulation. Previous studies have filtered the high-frequency modulation signal with a filter bandwidth fixed across all assessed modulation frequencies. As depicted in the present study, the consequence of an inappropriately narrow filter bandwidth is the unintentional elimination of the signal's amplitude modulation. If the high-frequency amplitude-modulated signal is either distorted or attenuated by the filter, then the CFC metric will not be accurate.

As depicted in the present study, a filter with appropriate bandwidth settings is necessary for preserving amplitude modulation and studying CFC. In particular, simulations are used to show that a filter with a bandwidth fixed for all assessed modulation frequencies produces false negatives at many modulation frequencies. This study proposes a method for filtering the high-frequency signal with a variable bandwidth that is designed to preserve amplitude modulation. This work applies basic signal processing methodology to improve the accuracy of the CFC metrics used to study brain function and connectivity. The use of simulated signals rather than real brain data allows an assessment of CFC methods, where the input signals are completely understood. Once the CFC methods are confirmed, these methods can be used to examine more complex brain recordings.

## Background Theory

Phase-amplitude CFC metrics seek to determine whether the amplitude or power of a high-frequency signal is modulated by the phase of a lower-frequency signal. An amplitude-modulated signal can be represented as follows:

$$S_{AM}(t) = (A + M \cdot \sin(2\pi f_m t + \phi_1)) \cdot \sin(2\pi f_c t + \phi_2) \quad (1)$$

where A is the offset constant, M is the amplitude, $f_c$ is the carrier radial frequency of the signal being modulated, and $f_m$ is the lower radial frequency of modulation. Variables $\phi_1$ and $\phi_2$ are the phases of the modulation and carrier signals, respectively. The sum of A and M determines the maximum possible value for the amplitude envelope, and the ratio of M to A determines the depth of modulation. Figures 1a–c provide an example of an amplitude-modulated signal. As shown in Figure 1d, the Fourier representation of this signal shows peaks at the carrier frequency and at the sidebands $\pm f_m$ centered at the carrier frequency.

Without sidebands at $f_c \pm f_m$, there is no amplitude modulation of the carrier signal. This is evident from the following identity, which uses the product-sum identity for sine waves:

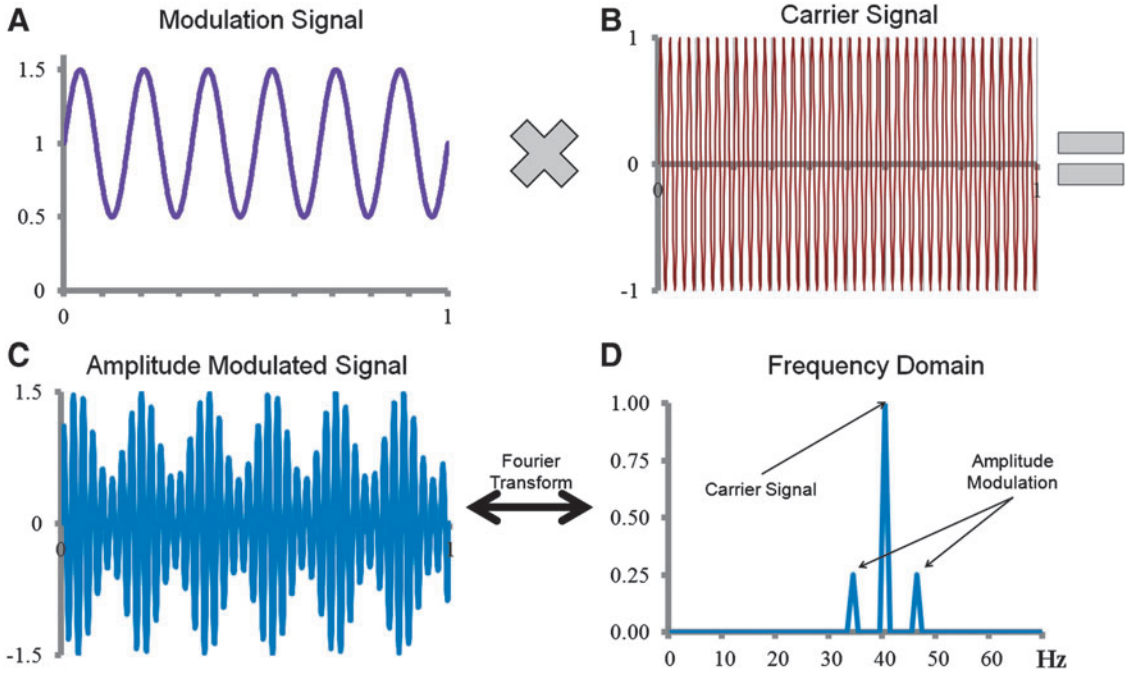


**FIG. 1.** Amplitude-modulated signal. **(A)** 6 Hz (modulation frequency, $f_m$) sine wave with an amplitude of 0.5, offset constant of 1, and phase offset ($\phi_1$) of zero is multiplied with **(B)** a 40 Hz (carrier frequency, $f_c$) sine wave with a phase offset ($\phi_2$) of zero. **(C)** The result is a 40 Hz sine wave amplitude modulated at 6 Hz with a depth of modulation equal to M/A = 0.5 or 50%. **(D)** The Fourier representation of the amplitude-modulated signal shows a peak at the 40 Hz carrier frequency, with sidebands at ± 6 Hz around the center carrier signal. Color images available online at www.liebertpub.com/brain

$$
\begin{aligned}
S_{AM}(t) &= (A + M \cdot \sin(2\pi f_m t)) \cdot \sin(2\pi f_c t) \qquad (2)\\
&= A \sin(2\pi f_c t) + \mathrm{M} \sin(2\pi f_m t) \sin(2\pi f_c t)\\
&= A \sin(2\pi f_c t)\\
&\quad + M \frac{(\cos(2\pi f_m t - 2\pi f_c t) - \cos(2\pi f_m t + 2\pi f_c t))}{2}\\
&= A \sin(2\pi f_c t)\\
&\quad + \frac{M}{2}(\cos(2\pi(f_m - f_c)t) - \cos(2\pi(f_m + f_c)t))\\
S_{AM}(t) &= A \sin(2\pi f_c t)\\
&\quad + \frac{M}{2}\left(\sin\left(2\pi(f_m - f_c)t + \frac{\pi}{2}\right) - \sin\left(2\pi(f_m + f_c)t + \frac{\pi}{2}\right)\right)
\end{aligned}
$$

As shown, the amplitude modulation of a signal is mathematically equivalent to adding signals with frequencies $f_c + f_m$ and $f_c - f_m$ to the carrier signal. It is this property that allows the information in a low-frequency signal to be encoded and transmitted with a high-frequency carrier wave. It is interesting to note that the frequency spectrum of the amplitude-modulated signal contains no power at $f_m$.

In phase-amplitude CFC, one seeks to measure the association between the phase of a low-frequency signal and the power of a high-frequency signal. In particular, one seeks to determine whether a measured signal is of the following form:

$$
\begin{aligned}
S_{rec}(t) &= S_{LFS}(t) + S_{AM}(t) + n(t) + r(t) \qquad (3)\\
&\textit{where, } S_{LFS}(t) = \sin(2\pi f_m t + \phi_1)
\end{aligned}
$$

The recorded signal $S_{rec}(t)$ containing CFC is represented as the summation of a low-frequency signal $S_{LFS}(t)$ and a high-frequency oscillation with amplitude modulation $S_{AM}(t)$. The noise term, n(t), includes sources from outside the brain and measurement error. The r(t) term includes unrelated brain signals. The CFC model assumes that low-frequency neuronal activity modulates the power of higher-frequency neural activity. The emphasis of this article is on the procedures used to determine the amplitude envelope of high-frequency brain activity.

## Methods

As shown in Figure 2, the general procedure that is used for computing phase-amplitude CFC metrics involves (1) obtaining the phase time series of a low-frequency band-passed signal; (2) determining the amplitude envelope of a high-frequency signal; (3) using a correlation measure that ascertains the dependence of the high-frequency amplitude envelope on the low-frequency phase, which is often expressed as the Modulation Index. Once the Modulation Index is computed, then a variety of methods are proposed for determining the statistical significance of this relationship. Phase and amplitude associations are often computed for many phase and amplitude pairs that are hypothesized as having a biological link, typically displayed as a comodulogram plot.

In the present study, brain signals were simulated and computed using Matlab (MathWorks, Natick, MA). Neuronal brain signals were simulated according to Equations 2 and 3 with A of 0.525 and M of 0.475. The phases, $\phi_1$ and $\phi_2$, as well as r(t) are zero. The simulated signal contains 60,000 points sampled at 500 Hz for 120 sec. Noise, n(t), is a zero-mean Gaussian. The CFC modulation index published by Canolty et al. (2006) was implemented in Matlab with fixed bandwidth filtering to extract the high-frequency, amplitude-modulated

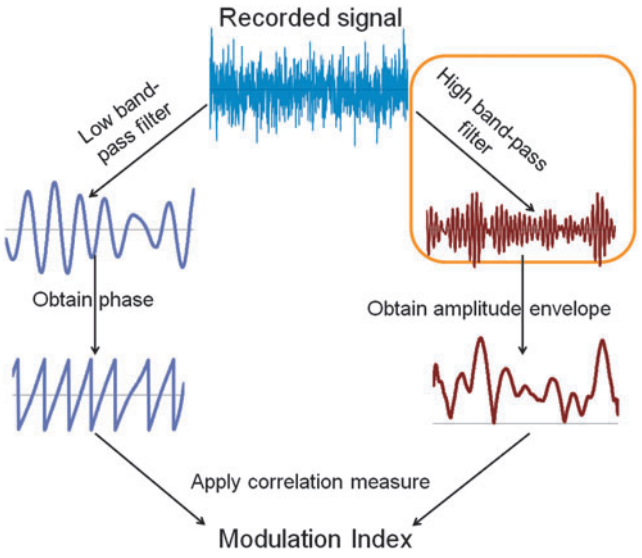


**FIG. 2.** Overall strategy for detecting phase-amplitude modulation in a recorded neuronal signal. The present study focuses on the high-frequency band pass filtering of the recorded signal. Color images available online at www.liebertpub.com/brain

signal. The fixed bandwidth filter follows the original implementation and filters the amplitude-modulated signal with a 4 Hz pass band centered on a defined carrier frequency. In addition, a variable bandwidth filtering method is introduced in this study to extract the high-frequency amplitude-modulated signal. The variable bandwidth filter uses a pass band of twice the modulation frequency that is hypothesized to modulate the carrier signal. Thus, the variable filter is designed to be inclusive of the sidebands about the carrier signal. Fixed and variable filtering was performed using the eegfilt function in the EEGLAB Matlab package (Delorme and Makeig, 2004). The filter order was set to 160 to reduce filter ripple and allow narrow filter transition bands. Fixed and variable filter parameters are detailed in Table 1.

The CFC method outlined in Osipova et al. (2008) was also implemented to study the effect of filter parameters. This CFC metric uses a sliding Fourier transform that estimates the instantaneous power of the high-frequency amplitude-modulated signal. In addition to implementing the standard Osipova et al. method, this method was modified with an option for varying the width of the time window. The number of signal cycles included in the time window controls the frequency resolution and, thus, the effective bandwidth.

For simulations, noise was added to examine the effect of noise on CFC measures. Signal-to-noise ratio (SNR) was calculated as the power of the low-frequency signal and the

Table 1. Pass-Band Limits for the Fixed and Variable Bandwidth Filters

| | *Pass-band definition* | |
|---|---|---|
| *Filter type* | *Lower limit* | *Upper limit* |
| Fixed BW | $f_c$ − 2Hz | $f_c$ + 2Hz |
| Variable BW | $f_c - f_m$ | $f_c + f_m$ |

BW, bandwidth; $f_m$, modulation frequency; $f_c$, carrier frequency.

high-frequency amplitude-modulated signal divided by the power of the added noise. SNR was changed by varying the standard deviation of the added Gaussian noise.

The described simulated signals and filters were used to perform three experiments with the aim of comparing the performance of the fixed bandwidth filter with the variable bandwidth filter. First, the two filter methods were used with signals amplitude modulated at three different frequencies. Second, the CFC metrics derived with the two filter methods were compared in the presence of the different signal noise levels. Third, comodulograms generated with the two filter methods were compared to examine the differences in sensitivity to CFC.

## Results

### *Performance of variable bandwidth filter*

Figure 3 demonstrates the Fourier spectrum of three phase-amplitude coupled signals, with low-frequency signals of 2, 6, and 10 Hz modulating a high-frequency signal of 40 Hz. The frequency spectrum of this signal contains four power peaks representing the singlet of $S_{LFS}(t)$, the center frequency of $S_{AM}$, and the two sidebands of $S_{AM}(t)$. The $S_{LFS}(t)$ signal is hypothesized to amplitude modulate the carrier frequency through CFC. For a better visualization of the frequency spectrum, the signal is multiplied by a Gaussian function to provide a width to peaks in the spectrum graph. Both the fixed and the variable high-frequency filters completely eliminate the low-frequency signals [i.e., in this case $S_{LFS}(t)$]. As shown in the center panels, the Fourier spectra of the filtered signal demonstrate that the 4 Hz fixed bandwidth filter results in no attenuation of the modulation sidebands at 2 Hz modulation. However, strong attenuation of the modulation sidebands is observed at 6 and 10 Hz. The 6 Hz modulation sidebands at 34 and 46 Hz are not fully attenuated by the fixed bandwidth filter, because the sidebands are within the transition band of the filter (see middle center panel). In contrast, the variable filter's band-pass range increases in width as the modulation frequency increases. Thus, as shown in the right panel of Figure 3, the variable bandwidth filter does not noticeably attenuate the sidebands. As shown in the next section, this property of the variable bandwidth filter preserves the amplitude modulation of $S_{AM}(t)$ and, thus, the possibility of observing CFC.

### *Filter design and the comodulation metric*

The impact of filter design on CFC was examined with different levels of signal noise. As shown in Figure 4, using the comodulation metric and statistics outlined in Canolty et al., (2006) a fixed bandwidth filter results in false-negative CFC values even at a high SNR (each data point represents the average of 100 simulations). The modulation index fails to reach significance ($p < 0.05$, uncorrected) for the 10 and 16 Hz modulations. The 6 Hz modulation achieves

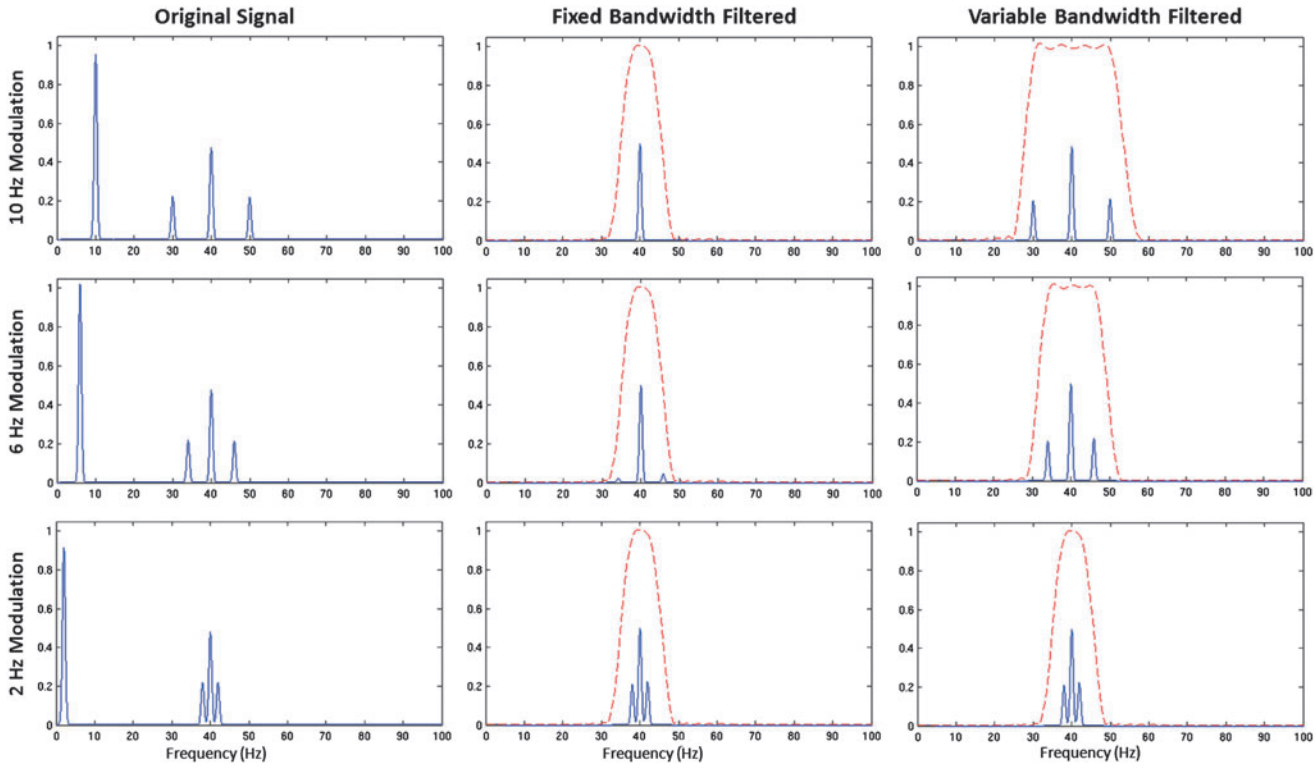


**FIG. 3.** Fourier spectrums of filtered and unfiltered phase-amplitude coupled signals. Fourier representations of phase-amplitude coupled sine waves at a carrier frequency of 40 Hz and amplitude modulations at 2, 6, and 10 Hz. The left column displays the frequency spectrum of the original signal. The central column shows the filter response of the fixed bandwidth filter (red) and the filtered signal (blue). The right column shows the filter response of the variable bandwidth filter (red) and the filtered signal (blue). The sidebands are preserved with the variable bandwidth filter at each modulation frequency. Color images available online at www.liebertpub.com/brain

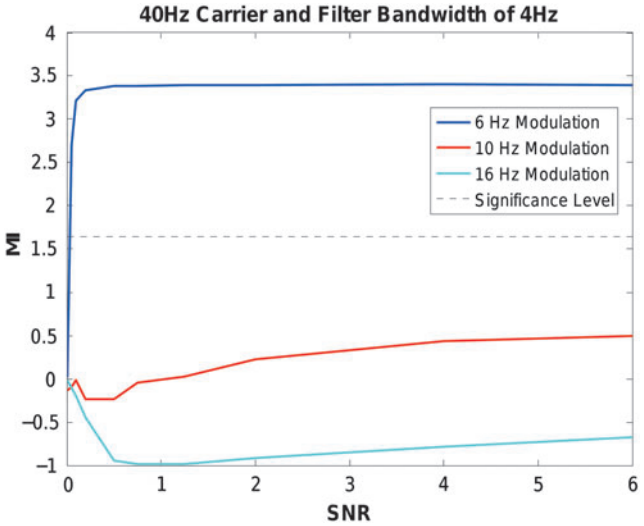


**FIG. 4.** Effect of using a fixed bandwidth filter width for computing CFC. Modulation Index values (y axis) for 40 Hz phase-amplitude coupled signals modulated at 6, 10, or 16 Hz over varying levels of SNR (x axis). A band pass filter with pass-band edge frequencies of 38 and 42 Hz was used, and each data point is the average of 100 simulations. Significance level is $p < 0.05$. CFC, cross-frequency coupling; MI, modulation index; SNR, signal to noise ratio.

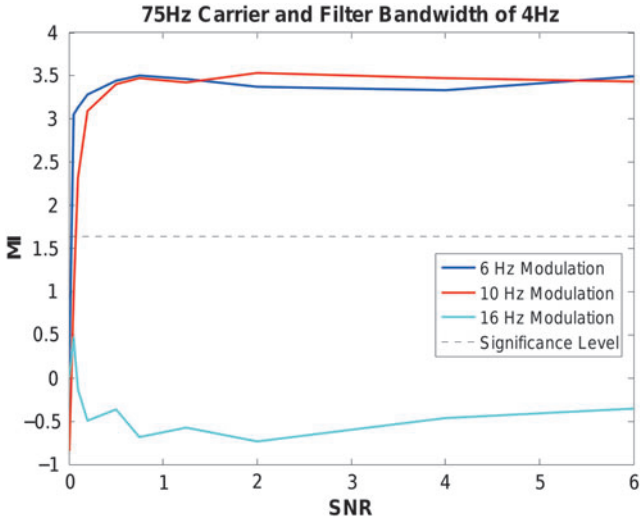


**FIG. 5.** Effect of wider transition bands at higher frequencies when computing CFC. Modulation Index values (y axis) for 75 Hz phase-amplitude coupled signals modulated at 6, 10, or 16 Hz over varying levels of SNR (x axis). A band pass filter with pass-band edge frequencies of 73 and 77 Hz was used, and each data point is the average of 100 simulations. Significance level is $p < 0.05$.

significance even at low SNRs. This is because although the low frequency modulation sidebands are outside the band-pass filter, the sidebands are still within the filter transition band (see Fig. 3, center row and column).

Transition band steepness impacted the sensitivity of the CFC metric. The EEGLab eegfilt function transition band default value is a fraction (15%) of the band-pass edge frequency. Thus, for frequencies such as high gamma (40 to 100 Hz), the transition band is relatively wide, resulting in less attenuation of neighboring frequencies containing sidebands. Figure 5 repeats the simulation of Figure 4, but with a carrier frequency of 75 Hz. In this case, the fixed bandwidth filter is centered at 75 Hz, with band-pass edge frequencies of 73 and 77 Hz. In this 75 Hz carrier signal example, a significant CFC of the 10 Hz modulation is observed at a relatively low SNR because the 10 Hz sideband lies within the transition bands and is not fully attenuated. This result is contrasted with the lack of significant CFC of the 10 Hz modulation and the 40 Hz carrier pair in Figure 4.

The simulation was repeated using the proposed variable bandwidth filter. Figure 6 shows the effect of taking the frequency of modulation into account and using the variable bandwidth filter for isolating the high-frequency activity. The modulation indices for the 6, 10, and 16 Hz modulations each reach significance given sufficient SNR. Only at extremely low SNR levels did the modulation index fail to detect phase-amplitude coupling.

### *High-frequency filtering and simulated comodulograms*

Figure 7 compares the performance of fixed and variable bandwidth filters using a comodulogram and the Canolty modulation index. The SNR of the simulated waveforms is 0.16. At a 6 Hz modulation, both filter methods detect amplitude modulations of the 40 Hz signal (left panel, Fig. 7). At a 10 Hz modulation, the fixed bandwidth method shows distinct and separate peaks at 45 and 35 Hz. In this case, the modulation index does not peak at 40 Hz, because the fixed band-pass filter does not include the 50 or 30 Hz sidebands. When centered at 40 Hz, the 4 Hz band-pass filter only extends from 38 to 42 Hz. As such, the filter produces a pure

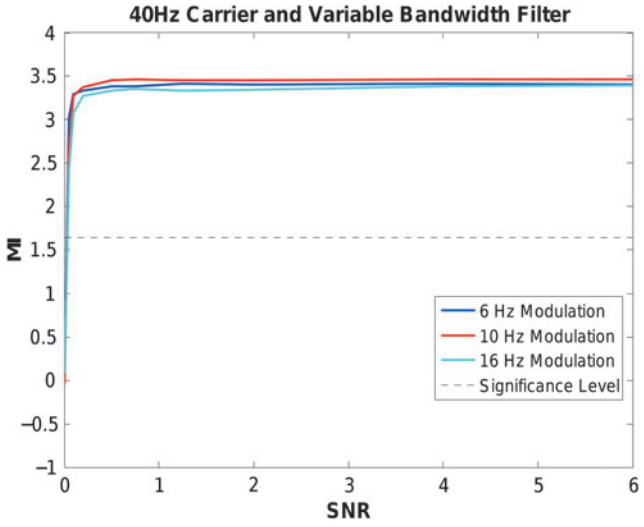


**FIG. 6.** Effect of using a variable bandwidth filter width when computing CFC. Modulation Index values (y axis) for 40 Hz phase-amplitude coupled signals modulated at 6, 10, or 16 Hz over varying levels of SNR (x axis). A band pass filter with pass-band edge frequencies of 34 and 46 Hz, 30 and 50 Hz, or 24 and 56 Hz was used, depending on the frequency of amplitude modulation. Each data point is the average of 100 simulations. Significance level is $p < 0.05$.

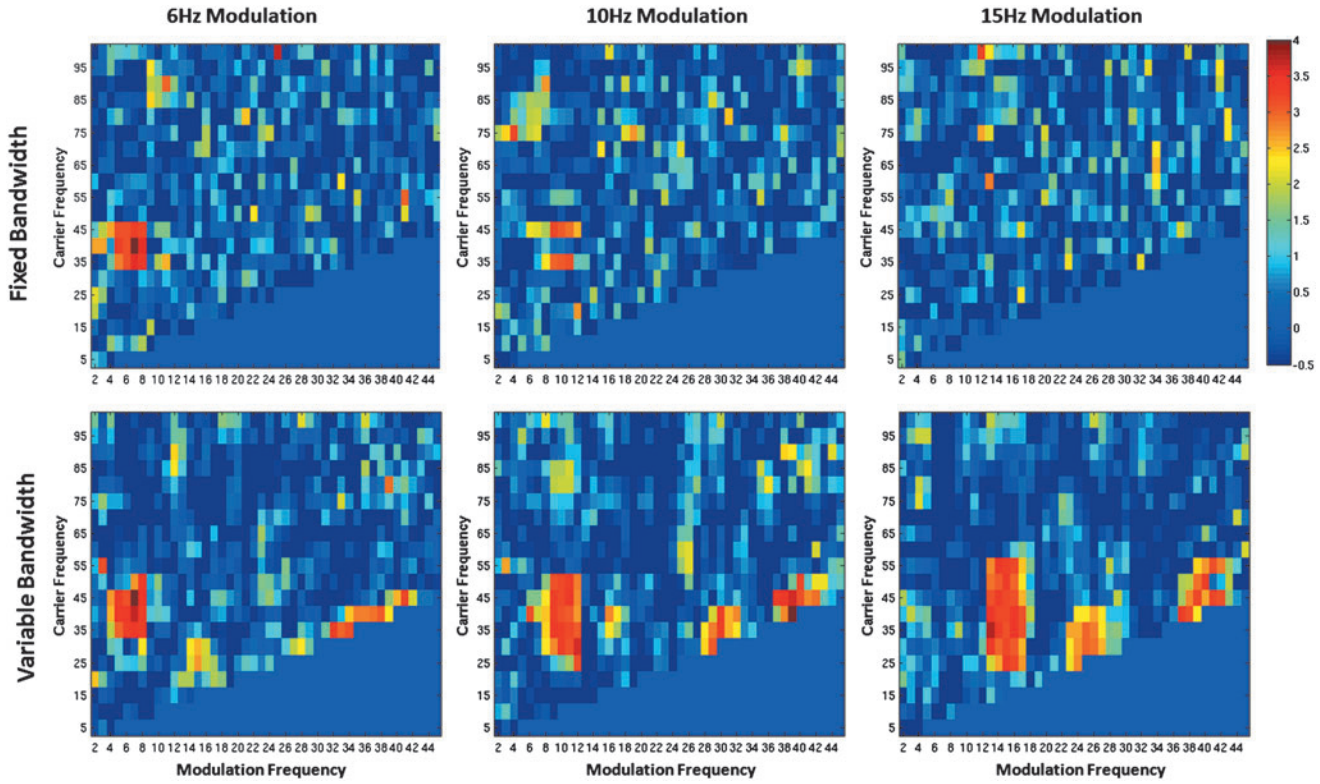


**FIG. 7.** Comodulograms showing the Canolty Modulation Index with fixed (top row) and variable (bottom row) bandwidth filters. The x axis shows the modulation frequency $f_m$, and the y axis depicts the carrier frequency $f_c$. Modulation frequencies of 6, 10, and 15 Hz are shown. Each filter technique detects the 6 Hz modulation (far left panel). Only the variable bandwidth filter, however, accurately detects the 10 and 15 Hz modulations.

sinusoidal signal of 40 Hz with no amplitude modulation. When CFC is measured for 35 or 45 Hz carrier frequencies, the fixed bandwidth filter pass band is between the center frequency and one of the sidebands. The fixed bandwidth pass band and transition band are of a sufficient width to include the center frequency and one of the sidebands. This produces a signal amplitude modulated at 10 Hz and, thus, comodulogram peaks at 35 and 45 Hz. At a 15 Hz modulation, the fixed bandwidth filter produces no large modulation indices, because the filter bandwidth is not wide enough at any point to include the center frequency and sideband.

The variable bandwidth filter detects amplitude modulation across all modulation frequencies (bottom row, Fig. 7). For example, at 10 Hz modulation, the variable bandwidth method shows a contiguous area of high modulation indices bounded by $\sim$50 and 30 Hz. The size of the region with high modulation indices increases with modulation frequency when the variable bandwidth filter is used. This is because the carrier frequency resolution decreases by increasing the filter bandwidth. Finally, it is also important to note the artifacts in the variable frequency comodulogram along the line where carrier frequency equals the modulation frequency.

Figures 8 and 9 demonstrate that the results observed with the Canolty modulation index extend to the Osipova coherence metric. The SNR of the simulated waveforms is 0.16. As the window size increases, the bandwidth of the sliding Fourier transforms decreases. Thus, as the width of the sliding Fourier window increases, the coherence metric becomes less sensitive to modulation. The slow modulation frequency of 6 Hz can be detected up to a window size of 40 cycles (Fig. 8). The faster modulation frequency of 15 Hz can only be detected up to a window size of 15 cycles (Fig. 9). The detection of the higher-modulation frequency requires a greater bandwidth than does the lower-modulation frequency.

## Discussion

As shown through simulations, CFC methods using inappropriate filter parameters can fail to detect real CFC for particular low-frequency phase and high-frequency amplitude pairs. This is because a narrow band-pass filter can eliminate the sidebands modulating a carrier frequency. The output of such a filter is a signal at the carrier frequency with no change in power or amplitude over time. Modulation frequencies at higher frequencies are most susceptible to this effect. Even a signal with high SNR will exhibit no significant cross-frequency modulation if the filter is poorly designed. In addition to the filter bandwidth, the width of the filter's transition zone from pass band to no-pass band was observed as having an impact on the sensitivity of the CFC metric. These results using the Canolty CFC metric were observed to extend to the Osipova modulation index, which uses a sliding Fourier transform that filters the high-frequency signals.

If a phase-amplitude relationship is hypothesized between two signals, then the high-frequency amplitude-modulated signal should be extracted with a sufficient bandwidth to preserve amplitude modulation. This study proposes a variable

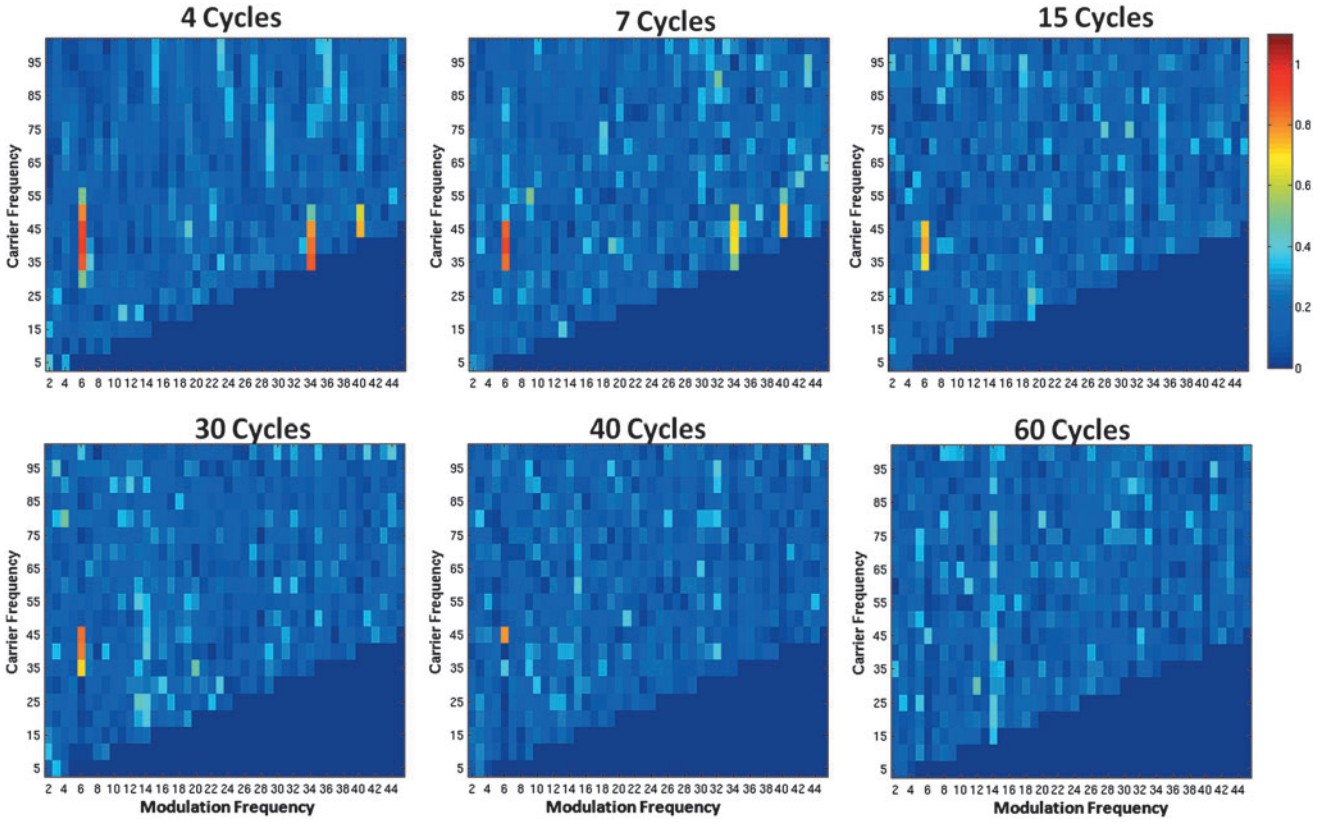


**FIG. 8.** Comodulograms showing the Osipova coherence metric with varying sliding Fourier transform window size. All panels use the same simulated 40 Hz high-frequency signal that is amplitude modulated by a 6 Hz signal. The x-axis shows the modulation frequency $f_m$, and the y axis depicts the carrier frequency, $f_c$. As the Fourier transform window size is increased (sizes 4 to 60 cycles), the sensitivity to CFC decreases.

bandwidth filter method that, by design, always contains sufficient bandwidth to include the modulating sidebands. This variable bandwidth filter increases the sensitivity to CFC at higher modulation frequencies. Amplitude modulations oscillating at frequencies between zero and the maximum bandwidth of the filter are retained for CFC assessment. In real data, it is expected that the amplitude-modulated sidebands will have broader spectral peaks than in simulated data. Such a modulation will still be detectable, as half the sideband's spectrum is within the pass band, and the other half is within the filter transition band.

As shown in Figure 7, the improved CFC sensitivity of the variable bandwidth filter results in a decreased carrier frequency resolution. The decrease in frequency resolution was observed as broadening the point-spread function around the true CFC peak on the comodulograms. The modulation frequency resolution is unaffected, because it is controlled by the bandwidth of the filter that is used to extract the low-frequency signal, $S_{LFS}(t)$. This filter has a narrow band pass, because $S_{LFS}(t)$ is not amplitude modulated.

It is important to note that CFC is only plausible for modulation frequencies less than the carrier frequency. For this reason, CFC measures on comodulograms should not be interpreted below the line where the carrier frequency equals the modulation frequency. In our variable bandwidth filter simulations, artifactual peaks in the comodulogram were observed along the line where carrier frequency equals the modulation frequency. This is because as the modulation frequency increases, the filter pass band will expand and eventually include the low-frequency modulation signals. If $f_c - f_m$ is less than $f_m$, the unintended consequence is to create a signal amplitude modulated at $f_c - f_m$ because of the inclusion of $S_{LFS}$. Given the constraint that $f_c - f_m > f_m$, comodulograms calculated with the variable bandwidth method should not be interpreted below the line $f_c = 2f_m$. This further constraint is caused by the filter's inability to separate the overlapping spectrums of $S_{LFS}(t)$ and $S_{AM}(t)$. If $S_{LFS}(t)$ and $S_{AM}(t)$ originate from distant cortices, then it may be possible to spatially separate the signals and measure CFC for modulation frequencies up to the carrier frequency.

In practice, most CFC studies have used filters with a fixed bandwidth in the order of 4 or 5 Hz. Such fixed settings are reasonable for examining how delta and theta signals (both less than or close to 4 Hz) modulate higher frequencies. As demonstrated in the present article, however, such settings are problematic when examining other frequency pairs. Specifically, the effects of high theta and alpha on high-frequency gamma activity cannot be accurately detected with a 4 Hz bandwidth filter.

The Osipova modulation index uses a sliding Fourier transform that isolates the high-frequency carrier signal of interest. This differs from the Canolty method, which uses a band-pass filter. The width of the Fourier time window is defined as a set number of cycles of the carrier frequency. Thus,

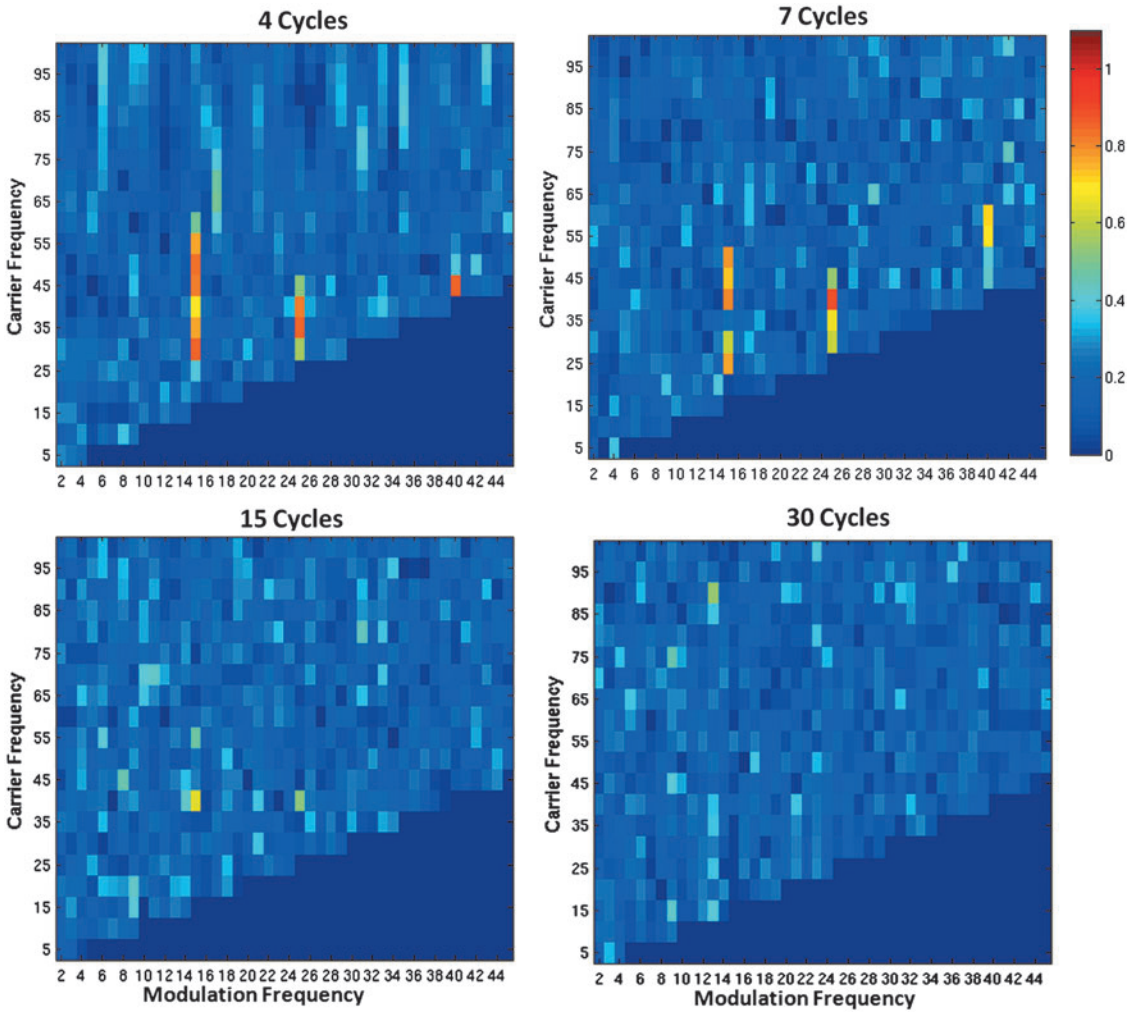


**FIG. 9.** Comodulograms showing the Osipova coherence metric by varying the sliding Fourier transform window size. All panels use the same 40 Hz high-frequency signal amplitude modulated by a 15 Hz signal. The x-axis shows the modulation frequency $f_m$, and the y axis depicts the carrier frequency $f_c$. CFC is barely detectable at a window size of 15 cycles and is not visible at a window size of 30 cycles.

the time window varies with carrier frequency, effectively changing the frequency resolution and bandwidth of the Fourier transform. As the time window is increased, the frequency resolution improves, and the effective bandwidth decreases. This study demonstrated that as the number of cycles within the time window increased, the modulation index became less sensitive to CFC. This decrease in sensitivity happens because the lower bandwidth prevents the modulation sidebands from being detected. Higher-modulation frequencies were observed as requiring shorter time windows for the CFC to be detectable. This phenomenon is conceptually identical to the sensitivity changes observed with the Canolty modulation index.

The simulations performed in this study represent a simple neural signal with no extraneous oscillations. Real measurements of brain electrophysiology contain noise and neuronal activity across the entire spectrum. In brain data, it is expected that in some instances unrelated signals will exist between the sideband frequency and the carrier frequency. Such a signal would also amplitude modulate the carrier signal if included after filtering. The detection of CFC in this case requires long measurement times and cross-frequency coupled signals of sufficient power. This study does not consider complex *in vivo* signals; however, the fundamental filtering requirements demonstrated in this study are at a minimum necessary to study real brain signals.

In addition to the considerations just mentioned, accurate, noninvasive EEG and MEG CFC and other FC measures are difficult to obtain for several reasons. Recordings from sensors placed on the scalp likely reflect the superposition of brain activity from multiple brain areas (shown in Equation 3). Given this superposition, the assessment of FC is optimally performed in source rather than sensor space (Hoechstetter et al., 2004; Nunez, 1997). Many source localization procedures, however, provide distorted amplitude and phase estimates of brain activity (Diwakar et al., 2011). Thus, in addition to the data analysis issues considered in this article, accurate estimates of CFC require accurate local measures of brain activity. For such analyses, source localization with MEG may be optimal, using single dipole, L1-minimum norm, and advanced beamforming methods (Diwakar et al., 2011; Hämäläinen and Ilmoniemi 1994; Huang et al., 2006; Mosher et al., 1992).

## Conclusion

In conclusion, this study applies the principles of signal processing to a current neuroscience application. CFC metrics are sensitive to the type of filter used to extract signals that are hypothesized to be biologically linked. Simulations showed that with fixed bandwidth filters, CFC was correctly estimated for theta-gamma but failed to reach significance for alpha-gamma and beta-gamma pairings, even at high SNRs. To avoid such type II errors, a modification to the standard method is proposed, such that the bandwidth of the high-frequency filter is a function of the amplitude modulation frequency. Simulations using this approach in the present study showed that correct CFC estimates were obtained for all 3 phase-amplitude pairings, even at low SNRs.

## Acknowledgments

This study was supported in part by NIH grant R01DC008871(T.P.R.), NIH grant R01DC008871-02S1(T.P.R.), NIH grant K08 MH085100(J.C.E.), and grants from the Nancy Lurie Marks Family Foundation (NLMFF). Additional support for the Neuroimaging Core was from Award number P30HD026979 from the Eunice Kennedy Shriver National Institute of Child Health & Human Development of the National Institutes of Health.

## Author Disclosure Statement

The authors report no competing financial interests pertaining to the work in the article.

## References

Axmacher N, Henseler MM, Jensen O, Weinreich I, Elger CE, Fell J. 2010. Cross-frequency coupling supports multi-item working memory in the human hippocampus. Proc Natl Acad Sci U S A 107:3228–3233.

Başar E, Başar-Eroglu C, Karakaş S, Schürmann M. 2001. Gamma, alpha, delta, and theta oscillations govern cognitive processes. Int J Psychophysiol 39:241–248.

Canolty RT, Cadieu CF, Koepsell K, Knight RT, Carmena JM. 2012. Multivariate Phase–Amplitude cross-frequency coupling in neurophysiological signals. Biomed Eng, IEEE Trans 59:8–11.

Canolty RT, Edwards E, Dalal SS, Soltani M, Nagarajan SS, Kirsch HE, Berger MS, Barbaro NM, Knight RT. 2006. High gamma power is phase-locked to theta oscillations in human neocortex. Science (New York, NY) 313:1626–1628.

Cohen MX. 2008. Assessing transient cross-frequency coupling in EEG data. J Neurosci Methods 168:494–499.

Delorme A, Makeig S. 2004. EEGLAB: an open source toolbox for analysis of single-trial EEG dynamics including independent component analysis. J Neurosci Methods 134:9–21.

Diwakar M, Tal O, Liu TT, Harrington DL, Srinivasan R, Muzzatti L, Song T, Theilmann RJ, Lee RR, Huang MX. 2011. Accurate reconstruction of temporal correlation for neuronal sources using the enhanced dual-core MEG beamformer. NeuroImage 56:1918–1928.

Fries P. 2005. A mechanism for cognitive dynamics: neuronal communication through neuronal coherence. Trends Cogn Sci 9:474–480.

Hämäläinen MS, Ilmoniemi RJ. 1994. Interpreting magnetic fields of the brain: Minimum norm estimates. Med Biol Eng Compu 32:35–42.

Handel B, Haarmeier T. 2009. Cross-frequency coupling of brain oscillations indicates the success in visual motion discrimination. NeuroImage 45:1040–1046.

Hoechstetter K, Bornfleth H, Weckesser D, Ille N, Berg P, Scherg M. 2004. BESA source coherence: a new method to study cortical oscillatory coupling. Brain Topogr 16:233–238.

Huang MX, Dale AM, Song T, Halgren E, Harrington DL, Podgorny I, Canive JM, Lewis S, Lee RR. 2006. Vector-based spatial-temporal minimum L1-norm solution for MEG. NeuroImage 31:1025–1037.

Kirihara K, Rissling AJ, Swerdlow NR, Braff DL, Light GA. 2012. Hierarchical organization of gamma and theta oscillatory dynamics in schizophrenia. Biol Psychiatry 71:873–880.

Mosher JC, Lewis PS, Leahy RM. 1992. Multiple dipole modeling and localization from spatio-temporal MEG data. IEEE Trans Bio-Med Eng 39:541–557.

Nunez P. 1997. EEG coherency I: statistics, reference electrode, volume conduction, laplacians, cortical imaging, and interpretation at multiple scales. Electroencephalogr Clin Neurophysiol 103:499–515.

Osipova D, Hermes D, Jensen O. 2008. Gamma power is phase-locked to posterior alpha activity. PloS One 3:e3990.

Sauseng P, Klimesch W, Gruber WR, Birbaumer N. 2008. Cross-frequency phase synchronization: a brain mechanism of memory matching and attention. NeuroImage 40:308–317.

Schoffelen JM, Poort J, Oostenveld R, Fries P. 2011. Selective movement preparation is subserved by selective increases in corticomuscular gamma-band coherence. J Neurosci: Off J Soc Neurosci 31:6750–6758.

Tallon-Baudry C, Bertrand O, Fischer C. 2001. Oscillatory synchrony between human extrastriate areas during visual short-term memory maintenance. J Neurosci: Off J Soc Neurosci 21:RC177.

Tort AB, Komorowski R, Eichenbaum H, Kopell N. 2010. Measuring phase-amplitude coupling between neuronal oscillations of different frequencies. J Neurophysiol 104: 1195–1210.

Tort AB, Kramer MA, Thorn C, Gibson DJ, Kubota Y, Graybiel AM, Kopell NJ. 2008. Dynamic cross-frequency couplings of local field potential oscillations in rat striatum and hippocampus during performance of a T-maze task. Proc Natl Acad Sci U S A 105:20517–20522.

Address correspondence to:
*Jeffrey I. Berman*
*Children's Hospital of Philadelphia*
*Department of Radiology*
*34th St. and Civic Center Blvd*
*Wood Building, Suite 2115*
*Philadelphia, PA 19104*

*E-mail:* bermanj@email.chop.edu